Coupled-channel results for atomic excitations in intermediate-energy heavy-ion collisions

Theo de Reus,* Udo Müller-Nehler,* and Gerhard Soff
Gesellschaft für Schwerionenforschung (GSI), D-6100 Darmstadt, Federal Republic of Germany

Joachim Reinhardt, Stefan Graf, Berndt Müller, and Walter Greiner
Institut für Theoretische Physik der J. W. Goethe Universität, D-6000 Frankfurt am Main, Federal Republic of Germany
(Received 17 January 1989)

Electron and positron emission spectra produced in heavy-ion collisions with beam energies in the range $E_{\rm lab}=8-100$ MeV/nucleon are calculated up to kinetic lepton energies of 50 MeV. Earlier predictions concerning the observability of nuclear stopping times in the range $\tau=1-10$ fm/c by means of the slope of δ-electron spectra are confirmed. However, the effect of time delay is somewhat less pronounced than predicted in first-order perturbation theory.

I. INTRODUCTION

One of the central questions in heavy-ion collisions at energies above the Coulomb barrier is the determination of nuclear reaction times. The theoretical description of experimentally measured quantities like fusion cross sections, distributions of fragment mass, charge, angular momentum and kinetic energy may be performed within the framework of several models. Among these, microscopic models based on the two-center shell model[1] or on the time-dependent Hartree-Fock prescription[2] and statistical models based on diffusion theory[3,4] are in widespread use. In both classes of models the physical quantities listed above depend crucially on the nuclear time delay ΔT. For a survey of different reaction models we refer to Refs. 5 and 6.

Calculations based on classical trajectories with friction[7–14] yield theoretical reaction times in the range of $\Delta T=10^{-21}$ s up to 5×10^{-21} s for collisions of very heavy ions. These times are too short in order to expect a clear signal for spontaneous positron emission[15–17] in supercritical systems with a total charge $Z>174$. Because of the modified nuclear kinematics, however, consequences are expected in the spectra of atomic δ electrons and atomic positrons as well as in K-hole formation: The reaction time ΔT causes a phase shift between the ionization amplitudes along the incoming and the outgoing branch of the trajectory relative to elastic collisions. Vice versa, conclusions can be drawn from modified δ-electron or positron spectra with respect to the underlying reaction times.[18–22]

These considerations lead to the concept of an atomic clock,[18,19] where nuclear reaction times are reflected by oscillations in δ-electron spectra with a width ΔE, that is inversely proportional to the delay time, $\Delta E=2\pi\hbar/\Delta T$. For short reaction times, $\Delta T\leq10^{-21}$ s, the first minimum is shifted to such high electron energies that the oscillations are usually not observable. However, the presence of the minimum still causes a measurable change[23–28] in the nearly exponential slope of the spectrum at smaller energies. In contrast to the minimum itself, the change in the slope is rather insensitive to fluctuations of the nuclear delay time ΔT which occur naturally due to averaging over impact parameter b or other relevant quantities. Hence, for deep-inelastic heavy-ion collisions at beam energies below 10 MeV/nucleon, the slope of the δ-electron spectrum has become a very successful measure of the nuclear reaction time.[23–28]

From a practical point of view there are two reasons to extend the calculations to higher lepton energies $E\gg1$ MeV. First of all, measurements of the δ-electron spectra in deep-inelastic collisions are now being performed up to kinetic energies of $E_{e^-}=8$ MeV. In this energy range oscillations are expected[29–31] even for reaction times of 10^{-21} s or shorter. Comparisons with theoretical results in this energy range could allow for a much more precise determination of nuclear reaction parameters.

Secondly, δ-electron spectra emitted in heavy-ion collisions at intermediate energies, $E_{\rm lab}=10-100$ MeV/nucleon, reach into much larger lepton-energy domains up to 50 MeV, as perturbative calculations have shown.[29,30] Experiments in this region, which will be soon feasible, can provide information on the dynamics of nuclear reactions on a time scale of $\Delta T=10^{-22}$ s or even less. This is the lower end of the range where collective behavior dominates nuclear motion. For even shorter times, electron-positron pair creation may still be a promising probe of the reaction dynamics, but it could be dominated by single-particle processes.

II. COUPLED-CHANNEL CALCULATIONS

A semiclassical method is used to describe the electron dynamics during the collision. It is based on the time-dependent two-center Dirac (TCD) equation ($\hbar=c=1$):

$$i\frac{\partial}{\partial t}\Phi_i[\mathbf{R}(t)]=H_{\rm TCD}[\mathbf{R}(t)]\Phi_i[\mathbf{R}(t)]\ , \tag{1}$$

where the Hamiltonian is given by

$$H_{\rm TCD}[\mathbf{R}(t)]=\boldsymbol{\alpha}\mathbf{p}+\beta m+V_{\rm TCD}(\mathbf{r},\mathbf{R})\ . \tag{2}$$

$V_{\rm TCD}(\mathbf{r},\mathbf{R})$ denotes the Coulomb potential for the two nuclear charge centers which includes the effects of finite

nuclear size and electron screening.[31] The electrons are treated relativistically and the time dependence is parametrized via the internuclear separation $\mathbf{R}(t)$. At nonrelativistic bombarding energies it is appropriate to expand the wave function Φ_i using the molecular eigenstates $\varphi_j[\mathbf{R}(t)]$ of $H_{\mathrm{TCD}}[\mathbf{R}(t)]$:

$$\Phi_i[\mathbf{R}(t)]=\sum_j a_{ij}(t)\varphi_j[\mathbf{R}(t)]\exp\{i\chi_j(t)\} , \tag{3}$$

with

$$\chi_j(t)=\int^t dt' E_j(t') . \tag{4}$$

We sum over bound states and integrate over continuum states of positive and negative energies, respectively. Inserting (3) into (1) and projecting with φ_k, we obtain a set of coupled differential equations for the complex occupation amplitudes $a_{ij}(t)$:

$$\dot{a}_{ij}(t)=-\sum_{k\neq j} a_{ik}\left\langle \varphi_j \left| \frac{\partial}{\partial t} \right| \varphi_k \right\rangle e^{i(\chi_j-\chi_k)} , \tag{5}$$

with the initial condition $a_{ij}(t=-\infty)=\delta_{ij}$. Splitting the time derivative $\partial/\partial t$ into a radial coupling $\dot{R}\partial/\partial R$ and a rotational coupling $i\omega\mathbf{J}$, the coupled equations (5) can be solved numerically.[31–34] In most calculations the monopole approximation[35] was used, where V_{TCD} is restricted to its spherically symmetric part and the rotational coupling is irrelevant. The differential probability dP/dE for emitting a δ-electron with energy E ultimately is given by Refs. 31–34

$$\frac{dP}{dE}=2\sum_{r<F}|a_{rp}|^2 , \tag{6}$$

where F is the Fermi level of the atomic system before the collision and p labels a particle state in the continuum with energy E.

To describe collisions incorporating nuclear reactions we previously employed two different friction model trajectories, introduced by Birkelund *et al.*[7–9] and by Schmidt *et al.*[10] Without going into detail we note as essential difference between these models the ratios between radial and tangential friction coefficients. Of immediate interest to us, however, is the resulting reaction time ΔT for U+U collisions at bombarding energies of about $E_{\mathrm{lab}}=10$ MeV/nucleon. Striking are the different reaction times ΔT in central collisions: According to Ref. 10 the time delay ΔT is about a factor of 10 greater than in the model proposed by Birkelund *et al.*

In Fig. 1(a) we display the calculated δ-electron spectrum for 10 MeV/nucleon U+U collisions employing the trajectory of Ref. 10, where essentially only radial friction occurs. The longest reaction times appear in central collisions and reach a value of $\Delta T=2.3\times10^{-21}$ s. For the impact parameters $b=0$ and 2 fm the spectra exhibit a steep decay until $E_{e^-}\simeq700$ keV. This point marks the beginning of oscillations with an energy width of $\Delta E\simeq1800$ keV. With increasing impact parameter b the starting point of oscillations is shifted towards higher kinetic electron energies, since larger values for b are correlated with shorter reaction times ΔT in this model.

At first sight nothing fundamentally new can be learned by studying positron emission in deep inelastic heavy ion reactions. Considering collisions with a total nuclear charge $Z>174$, however, might be conducive in finding an alternative approach to an experimental detection of spontaneous positron production.[15–17] Figure 1(b) shows coupled-channel results for positron emission in deep inelastic U+U collisions at a bombarding energy of $E_{\mathrm{lab}}=10$ MeV/nucleon. Again, we have considered trajectories including nuclear friction according to model,[10] yielding an appropriate reaction time, as we learned

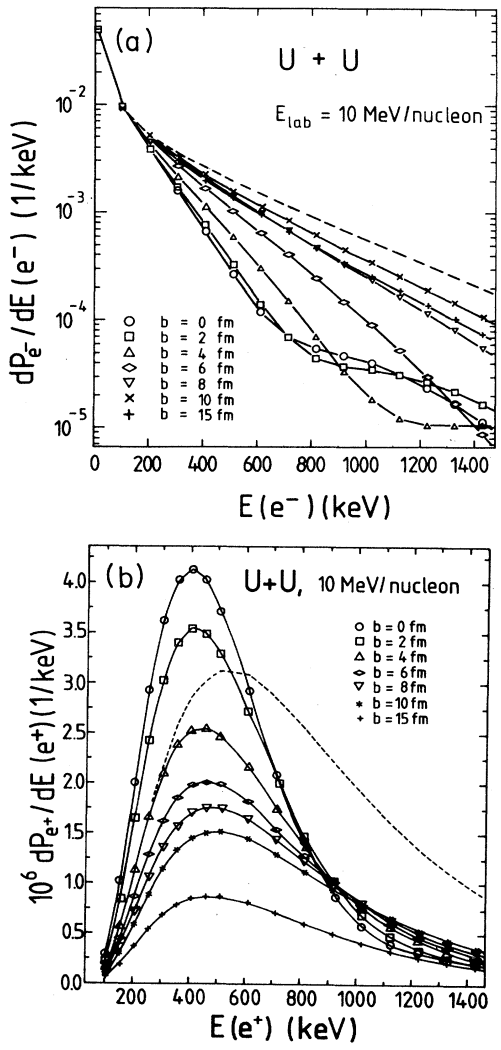

FIG. 1. (a) Electron emission in deep inelastic U+U collisions at $E_{\mathrm{lab}}=10$ MeV/nucleon. The considered impact parameters are $b=0$, 2, 4, 6, 8, 10, and 15 fm. The dashed curve shows a calculation for the case of elastic Rutherford scattering in a central collision, i.e., $b=0$. Employing the trajectory model of Ref. 10, clear signatures for oscillations are visible for small impact parameters $b=0$, 2, 4 fm. Delay times ΔT of up to 2.3×10^{-21} s are predicted in this model for central collisions. (b) Coupled-channel calculations for positron emission in deep-inelastic U+U collisions for the same nuclear dynamics. The dashed curve displays the result for a central elastic collision assuming pointlike nuclei.

from the experimental data.[23–28] The total spectra displayed in the figure are composed of s- and $p_{1/2}$-channel positron emission. For reasons of comparison we also have shown the result for elastic Rutherford scattering in a central ($b=0$) collision, displayed by the dashed curve. In case of $p_{1/2}$-positron emission the spectrum consists solely of dynamically emitted positrons, due to the time varying Coulomb field. Destructive interferences between the incoming and the outgoing branch of the friction model trajectory cause the appearance of spectra with emission probabilities notably below values obtained in elastic scattering. The same argument holds true for the s channel if spontaneous positron emission would be omitted. Especially the curves for small impact parameters $b=0$, 2, and 4 fm, where comparatively long reaction times occur, contain a considerable fraction of spontaneous positrons. Employing this argument the ratio

$$\frac{\int_{b=0}^{b_f} dP_{e^+}^{s+p}/dE_{e^+} bdb}{\int_{b=0}^{b_f} dP_{e^+}^{p}/dE_{e^+} bdb}$$

can be considered for sufficiently small impact parameters. The differential emission probability $dP_{e^+}^{s+p}/dE_{e^+}$ contains also spontaneous positrons, whereas the same quantity neglecting the vacuum decay is approximated by $2dP_{e^+}^{p}/dE_{e^+}$. Considering the system U+U at $E_{\rm lab}=10$ MeV/nucleon displayed in Fig. 1(b), this ratio increases from 1.3 to 2.3 for kinetic positron energies in the range $E_{e^+}=200$–800 keV when using $b_f=4$ fm and hence yields an alternative tool to detect spontaneous positrons.

Obviously only reaction times $\Delta T \leq 2\times 10^{-21}$ s are realized in the collisions considered so far, with the consequence that oscillation patterns have a width of more than 1000 keV. However, we may make a virtue of necessity by extending our calculations to electron energies $E_{e^-}>1$ MeV. We defer the discussion of how this is done technically to the corresponding section, where intermediate energy collisions are discussed. These extended calculations are not purely of theoretical interest but are necessary to describe recent experiments in which δ-electron emission has been measured for electron energies up to $E_{e^-}=2500$ keV, e.g., in 8.6 MeV/nucleon U+Au collisions.[26] Furthermore experimentalists are planning to extend the detections up to electron energies of $E_{e^-}=10$ MeV and even beyond.

Until now the extended coupled-channel code is available only for subcritical collision systems, i.e., where the binding energy of the $1s\sigma$ state remains located within the particle-antiparticle gap, although, there is no fundamental difficulty to extend the code also for supercritical collisions. For this reason we consider the heaviest system, still remaining subcritical for central collisions at a bombarding energy of $E_{\rm lab}=8.4$ MeV/nucleon, when using the friction model trajectory according to Schmidt, Wolschin *et al.*[10,14] In Fig. 2 we display data obtained from the extended coupled-channel code for the system Th+Pb at $E_{\rm lab}=8.4$ MeV/nucleon. Differential emission probabilities of δ electrons for kinetic electron energies $E_{e^-}<10$ MeV are displayed for impact parameters $b=0$–6 fm. Only small oscillations having widths varying between $\Delta E=1.8$ MeV and $\Delta E=6$ MeV are predicted by our calculations. These oscillations are more pronounced for the $p_{1/2}$ channel alone, being associated with a stronger relative variation of the inner-shell molecular $p_{1/2}$ states as function of the internuclear distance R. For the displayed spectra we have listed the energy width ΔE of the oscillations and the corresponding reaction time ΔT in Table I as function of the impact parameter b. Since the starting point of the oscillations varies in dependence on the impact parameter between $E_{e^-}\simeq 1$

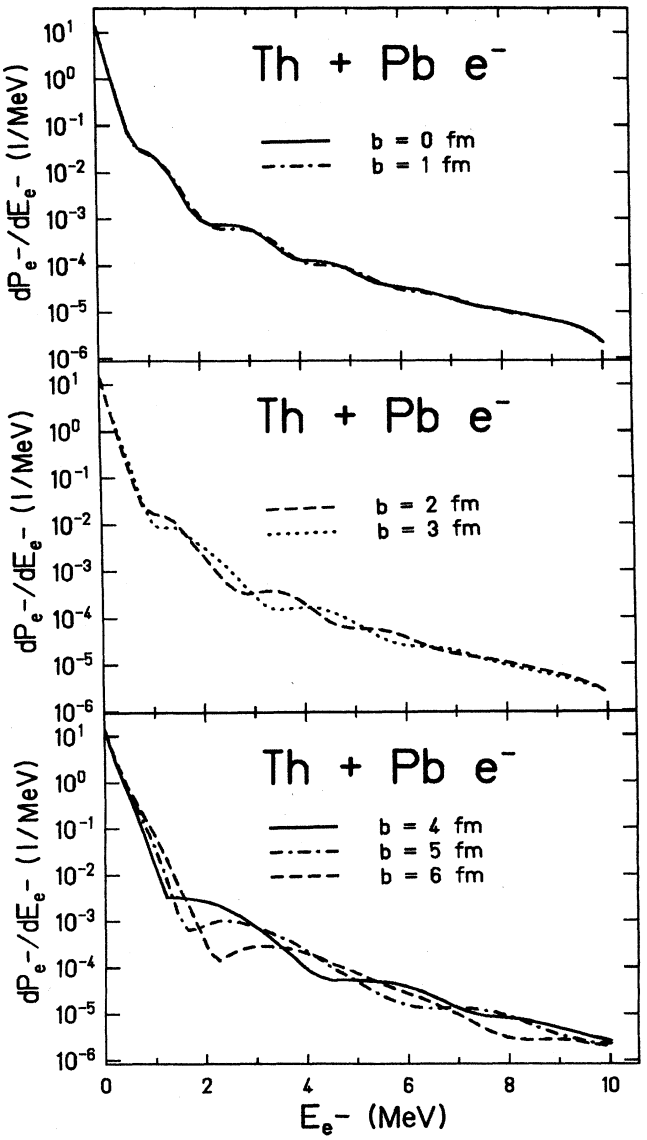

FIG. 2. Results of the extended coupled-channel code for δ-electron emission from 8.4 MeV/nucleon Th+Pb collisions. The calculations have been carried out for the impact parameters $b=0$, 1 (upper part), 2, 3 (middle part), 4, 5, and 6 fm (lower part) again employing the classical friction trajectories of model.[10] The total spectra are shown, which consist of the incoherent sum of s- and $p_{1/2}$-channel results. $F=3s\sigma,4p_{1/2}\sigma$.

TABLE I. Reaction times ΔT and widths ΔE for 8.4 MeV/nucleon deep-inelastic Pb+Th collisions. According to $\Delta E = 2\pi\hbar/\Delta T$ the reaction time ΔT can be determined by means of the energy width ΔE associated with the oscillations in δ-electron spectra.[18,19] We have applied this procedure to Fig. 2 and obtain values ΔT for the reaction time being in agreement with data extracted from the friction model trajectory[10,14] of Schmidt, Wolschin *et al.*

b (fm)	ΔE (MeV)	ΔT (10^{-21} s)
0	1.76	2.34
1	1.83	2.25
2	2.20	1.87
3	2.64	1.56
4	3.08	1.34
5	4.41	0.94
6	5.90	0.70

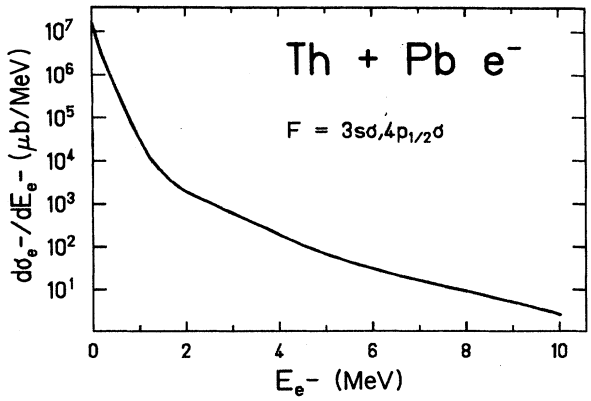

FIG. 3. Differential cross section for δ-electron emission in Th+Pb collisions at a beam energy of $E_{\rm lab} = 8.4$ MeV/nucleon. The data are obtained by integrating the differential emission probabilities shown in Fig. 2 over an impact parameter range of $b = 0$ to 6 fm. Oscillations being visible for the individual impact parameters vanish, instead a bend in the range 1 MeV $\leq E_{e^-} \leq$ 2 MeV and a change in the slope remains.

MeV and $E_{e^-} \simeq 2$ MeV, and furthermore, since the wiggles exhibit different energy widths ΔE, they vanish when performing an integration over impact parameters b. The result of such an integration in the limits $b = 0$ to 6 fm is displayed in Fig. 3. What remains is a bend in the slope of the spectrum between 1 MeV $\leq E_{e^-} \leq$ 2 MeV. Thus there is almost no chance to detect the oscillations experimentally, unless one might be able to select collisions associated with a sufficiently narrow impact parameter range Δb. However, even in this unlikely case there is still the fundamental dispersion of the reaction time due to quantal and statistical fluctuations. These also tend to smear our oscillations in the δ-electron spectrum.

III. COUPLING MATRIX ELEMENTS AT HIGH ENERGIES

Before we discuss the coupled-channel results for δ-electron and positron emission in intermediate-energy heavy-ion collisions, some preliminary remarks concerning the matrix elements

$$M_{ij} = \left\langle \varphi_i \left| \frac{\partial}{\partial R} \right| \varphi_j \right\rangle = \frac{1}{E_j - E_i} \left\langle \varphi_i \left| \frac{\partial V_0}{\partial R} \right| \varphi_j \right\rangle , \tag{7}$$

which enter into the coupled-channel equations (5), are necessary. In previous numerical calculations for K-vacancy formation, δ-electron and positron emission in collisions at beam energies in the vicinity of the Coulomb barrier only continuum states with energies up to 3 MeV were taken into account. However, in 20–100 MeV/nucleon collisions the high energetic tail of δ-electron spectra is of special interest, since it promises to exhibit a strong sensitivity on the stopping time τ. This can be understood by considering the scaling law derived in Ref. 30 within the framework of first-order time-dependent perturbation theory

$$\frac{dP_{e^-}}{dE_{e^-}} \simeq N^2(E, Z_{\rm tot}) \left\{ \left[\frac{\pi}{2\gamma} \right]^2 \exp\left[-\frac{\Delta E}{\hbar}(R_m/v_\infty + \pi\tau/2) \right] + \frac{2\pi^2(1+\frac{1}{2}\pi\alpha^2)^2}{\gamma f(\alpha,\beta)} \exp\left[-\frac{\Delta E}{\hbar}\left[\frac{R_m}{2v_\infty} + \frac{3}{4}\pi\tau \right] \right] \right.$$
$$\left. + \frac{(2\pi)^2(1+\frac{1}{2}\pi\alpha^2)^4}{f^2(\alpha,\beta)} \exp\left[-\frac{\Delta E}{\hbar}\pi\tau \right] \right\} , \tag{8}$$

where $\alpha = \Delta E\tau/2\hbar$, $\beta = R_m \Delta E/(\hbar v_\infty)$, $\gamma = 2R_m/(\tau v_\infty)$, and $f(\alpha,\beta) = (2\beta)^2 + (\alpha \ln 2)^2$. R_m indicates the position of the maximum in the coupling matrix element, being in the vicinity of the contact point $R_{\rm cont}$ of the two nuclei. $N(E, Z_{\rm tot})$ is a normalization factor being only weakly dependent on the involved continuum energy E_{e^-} and v_∞ is the initial heavy-ion velocity. Short stopping times τ correspond to high electron energies $E_{e^-} \sim 1/\tau$. For this reason matrix elements including high energy continuum states are required. The problem here is that numerical calculations exhibit oscillations in the matrix elements as function of the two-center distance R, starting at $R < 50$ fm for sufficiently high continuum energies. These oscillations reflect the shape of continuum wave functions for high electron or positron energies.

In order to explain this we make use of an approximate analytic expression for the matrix elements $\langle f | \partial/\partial R | i \rangle$, which may be evaluated by replacing the wave functions with solutions of free particles.[36] This procedure appears reasonable for continuum wave functions with sufficiently high energy

$$\Psi_\kappa^\mu = N_\kappa^\mu \begin{pmatrix} j_l \chi_\kappa^\mu \\ \dfrac{ipS_\kappa}{W+1} j_{\bar{l}} \chi_{-\kappa}^\mu \end{pmatrix} \tag{9}$$

where

$$l=\kappa \text{ for } \kappa>0, \quad l=-\kappa-1 \text{ for } \kappa<0 ,$$

and

$$\bar{l}=\kappa-1 \text{ for } \kappa>0, \quad \bar{l}=-\kappa \text{ for } \kappa<0 .$$

$p=(W^2-1)^{1/2}$ and S_κ indicates the sign of κ. N_κ^μ is a normalization constant. In (9) j_l signify spherical Bessel functions and χ_κ^μ denote spherical spinors.[36] For the derivative of the two-center potential in the monopole approximation, its value for the interior region is taken

$$\frac{\partial V_o}{\partial R} = \frac{2Ze^2}{R^2} \Theta(R/2-r) . \tag{10}$$

The energy $W=E-V_0$ in Eq. (9) can be replaced by $W \simeq E$ for $|E| \gg m$, so that the evaluation of the matrix elements reduces to

$$M_{ij} = \frac{1}{E_j-E_i} \int_0^{R/2} \Psi_i^+ \frac{2Ze^2}{R^2} \Psi_j d^3r . \tag{11}$$

The integral (11) can easily be solved analytically. For example, in the limit of large two-center distances R and high continuum energies E, the following expression is obtained for the radial coupling matrix elements between the continuum states φ_{E_i} and φ_{E_j}

$$\frac{1}{E_j-E_i} \left\langle \varphi_{E_i} \left| \frac{\partial V_0}{\partial R} \right| \varphi_{E_j} \right\rangle \sim \sin \left[\frac{p_j-p_i}{2} R + \delta_{E_i,E_j} \right] . \tag{12}$$

The electron momentum p thus determines the width of the oscillations in the matrix elements.

As an example for the applicability of Eq. (12) we consider the matrix element for the transition of a $1s\sigma$ electron into the state $E_{e^-}=40\, m_e c^2$ in the Dirac continuum of positive frequencies. In Fig. 4(b), a wavelength of $\lambda=121$ fm can be deduced, precisely agreeing with the analytical result similar to Eq. (12). According to this equation the oscillation frequency increases about linearly with the continuum energy for sufficiently large values. In this range expressions similar to Eq. (12) yield quantitative correct values for the wavelength, whereas discrepancies arise when continuum states with small energies are involved.

Due to the variation of the first zero with continuum energy, a fixed grid point distribution is no longer appropriate for the tabulation of the matrix elements as function of R. For this reason each matrix element carries an individual grid point distribution in our extended coupled-channel code. At least 29 values are stored in a logarithmic distribution on R for each matrix element until the first zero. For larger values the numerically achieved results are fitted according to Eq. (12), so that the matrix elements can be expressed analytically for large two-center separations R.

We note that a certain care is required when integrating the system of coupled-channel equations (5) for high continuum energies. Due to the high Fourier frequencies involved, sharp bends of the integrand may generate artificial numerical oscillations in the calculated spectra of electron or positron emission. We have found that a cubic spline interpolation yields sufficiently smooth curves between the interpolation points.

In order to check the quality of the new extended coupled-channel code with respect to the modified interpolation and extrapolation routines, we performed a calculation for δ-electron emission in the system Pb+Pb at a bombarding energy of $E_{\rm lab}=5.9$ MeV/nucleon. The dashed curve in Fig. 5 displays the result of the extended code, which is in excellent agreement with previous results although considerably fewer grid points on the energy scale have been used.

For beam energies beyond 10 MeV/nucleon, nuclear scattering is highly inelastic, especially for small impact parameters b. For our purposes we describe the nuclear trajectory in the framework of a classical friction model

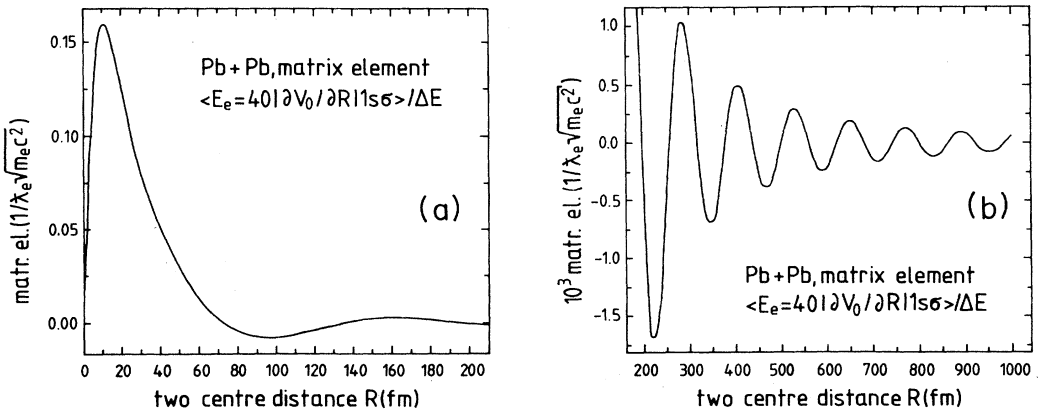

FIG. 4. Matrix element for the transition of a $1s\sigma$ electron into the continuum state $E_{e^-}=40\, m_e c^2$ as function of the two-center distance R in the system Pb+Pb. The numerically evaluated matrix element exhibits oscillations with a wavelength λ being inversely proportional to the electron momentum p. From part (b) of the figure a value of $\lambda=121$ fm can be deduced.

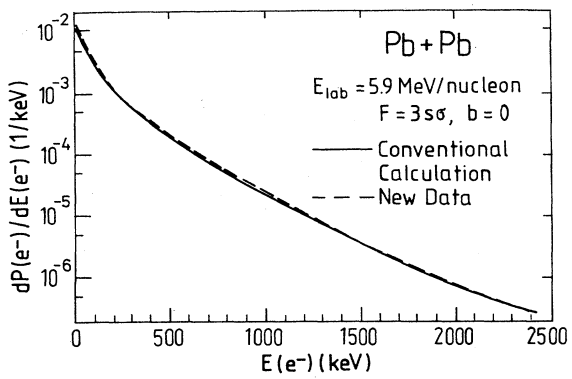

FIG. 5. Emission of δ electrons with angular momentum quantum number $\kappa=-1$ in central Pb+Pb collisions at a beam energy of $E_{\rm lab}=5.9$ MeV/nucleon. The full curve shows the results of previous calculations including 15 grid points in the energy range up to $E_{e^-}=6m_ec^2$. The dashed curve is obtained by the new, extended code, using only four points in the same range at the energies $E_{e^-}=1.02$, 1.5, 2, and 4 m_ec^2.

as outlined in Ref. 37. According to this model the friction force is proportional to the nuclear overlap region and also to the relative nuclear velocity. The Stokes-type friction coefficient is labeled by K. For the Coulomb part of the interaction potential the authors of Ref. 38 applied molecular harmonic oscillator (MHO) densities, whereas the nuclear potential has been evaluated within the energy-density formalism according to Ref. 39 by using the sudden approximation. In calculations for photon and pion radiation the classical friction model mentioned above has yielded satisfactory results.[38] Table II displays typical values for the stopping times τ in dependence on beam energy and friction coefficient K. We have defined the stopping time τ as follows: for example, the velocities displayed in Fig. 6(a) are approximated by

$$v(t)=\frac{v_0}{1+\exp\left[\dfrac{t-t_0}{\tau}\right]} .$$

TABLE II. Stopping times τ for central collisions obtained by the classical friction model as described in Ref. 37 for the system Pb+Pb. The data are listed in dependence on bombarding energy $E_{\rm lab}$ and friction coefficient K.

$E_{\rm lab}$(MeV/nucleon)	K(MeV fm^2)	τ(fm/c)
20	2500	8.7
20	5000	7.1
20	10000	6.2
60	2500	4.5
60	5000	3.6
60	10000	3.1
100	2500	3.4
100	5000	2.8
100	10000	2.3

At $t=t_0$ the velocity has reached half of its value of its offset, thus the stopping time τ is defined according to

$$\tau=-\frac{v_0}{4\dot{v}(t_0)} .$$

With increasing values of the friction coefficient K the deceleration for central collisions becomes more abrupt and hence the distance of closest approach at nulear overlap decreases. As a specific example we show in Fig. 6 the velocity and the two-center distance R as functions of the collision time for the system Pb+Pb at $E_{\rm lab}=60$ MeV/nucleon and $K=5000$ MeV fm^2 at different impact parameters b.

For the numerical evaluation of δ-electron spectra at intermediate bombarding energies we use a classical Rutherford trajectory down to a two-center distance of $R=30$ fm. Subsequently we append the trajectory resulting from the friction model described above. Concerning the exit channel of the collision no unique path can be predicted since an undetermined number of fragments will result for values of the impact parameter $b<b_{\rm grazing}$. Fortunately, the explicit knowledge of the outgoing trajectory is not required for the high energetic tail of δ-electron or positron spectra. This part of the spectrum is

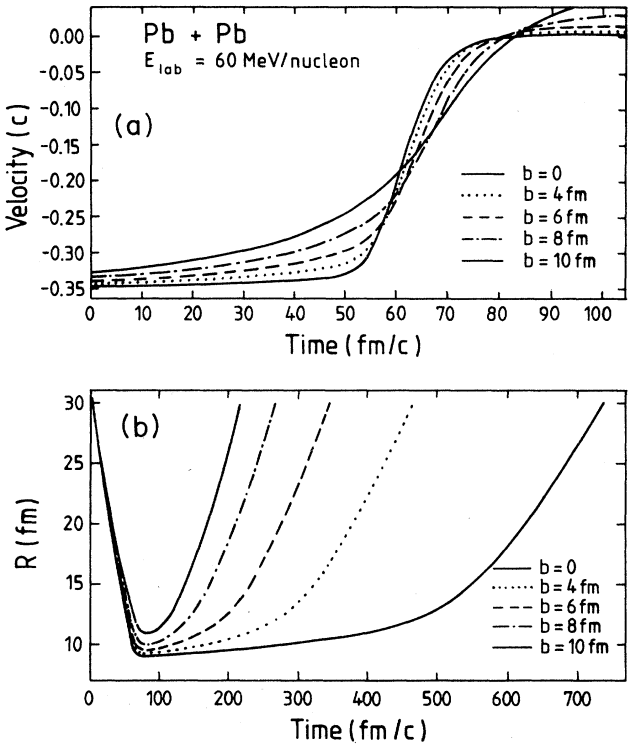

FIG. 6. (a) Velocity profile in 60 MeV/nucleon Pb+Pb collisions versus collision time t as function of different impact parameters $b=0$, 4, 6, 8, and 10 fm for a friction coefficient $K=5000$ MeV fm^2. The stopping time increases with rising values for b. Part (b) displays the corresponding two center distances as function of the collision time. With increasing impact parameter b the value of $R_{\rm min}$ rises, the time delay ΔT or reaction time, respectively, however, decreases.

determined entirely by the dynamics in the internuclear collision zone. To be specific, we found that the leptonic emission spectra for energies $E_{e^\pm} > 10$ MeV are invariant when performing calculations with a full outgoing Rutherford trajectory or, alternatively, using the amplitudes obtained by artificially cutting off the collision. In contrast δ-electron or positron spectra for kinetic lepton energies $E_{e^\pm} < 10$ MeV depend on the explicit shape of the exit channel and show oscillations which are a measure of the reaction time. Omittance of the outgoing trajectory yields exponentially decreasing spectra also for this region.

The invariance of the high energetic wing of δ-electron spectra with respect to the exit channel can also be recognized from Fig. 7. The real part of the differentiated transition amplitude $\dot{a}_{1s\sigma,E}(t)$ for an electron being ionized from the $1s\sigma$ state to continuum states with positive energies $E_{e^-}=24$ MeV and $E_{e^-}=50$ MeV, respectively, is plotted versus the collision time. For the considered central 60 MeV/nucleon Pb+Pb collision the deceleration occurs between $t=-0.5\lambda_e/c$ until $t=0$. Roughly speaking, the time integration of the coupled-channel equations (9) obtains its main contribution for the amplitudes $a_{1s\sigma,E}(t)$ before $t=0$, when high continuum energies $E_{e^\pm}$ are considered. Beyond this value, until $t=+\infty$ the integrand approximately averages to zero.

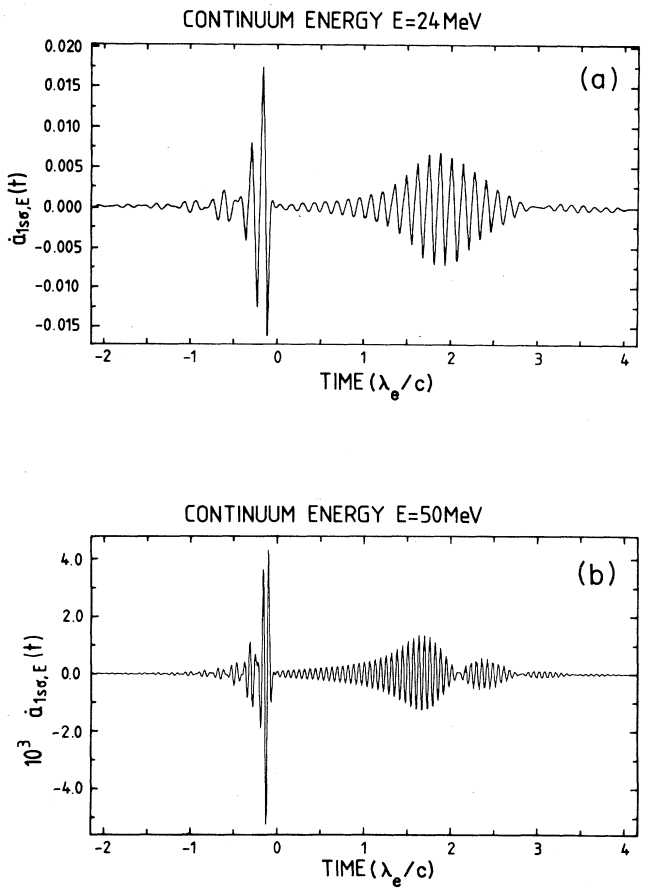

FIG. 7. (a) Real part of the differential transition amplitude $\dot{a}_{1s\sigma,E}(t)$ for $E_{e^-}=24$ MeV in a central $E_{\rm lab}=60$ MeV/nucleon Pb+Pb collision. Note that the maximum height of the amplitude at $t\simeq -0.15\ \lambda_e/c$ coincides with maximum deceleration of the internuclear velocity $\dot{R}$. Part (b) shows the same for a continuum energy $E_{e^-}=50$ MeV. The ratio of $|\dot{a}_{1s\sigma,E}(t=-0.15\ \lambda_e/c)|/|\dot{a}_{1s\sigma,E}(t=1.5-2\lambda_e/c)|$ increases with increasing continuum energy E_{e^-}.

In our numerical calculations for the emission probabilities of high energetic electrons and positrons at intermediate bombarding energies we took into account eight bound states for the s channel, six bound states for the p channel, and for each partial wave, 50 states in the upper and lower continuum, respectively. The grid points for continuum energies have been distributed logarithmically in the extended coupled-channel code. With increasing energy E_{e^-} or E_{e^+} thus an energy interval with a width up to $\Delta E=3$ MeV at $E_{e^\pm}=50$ MeV is characterized by one state.

IV. RESULTS FOR INTERMEDIATE ENERGIES

We now present some results for the system Pb+Pb at intermediate bombarding energies. Although the exit channel is unknown for sufficiently small impact parameters b, we have assumed two-body kinematics described by a Rutherford trajectory. Hence oscillations show up in the energy range $E_{e^-}\leq 10$ MeV caused by interference effects. The latter reflect reaction times on the scale $1-2\times10^{-21}$ s and generate oscillations with a width $\Delta E\simeq 2-3$ MeV. According to our calculations the main contribution to the emission of high energetic electrons or positrons results from the $s\sigma$ channel yielding about a factor of 10 higher emission probabilities compared to the $p_{1/2}\sigma$ channel.

Figure 8 shows for central Pb+Pb collisions the dependence of the δ-electron emission probabilities on the bombarding energies of $E_{\rm lab}=20$, 60, and 100 MeV/nucleon. Increasing the beam energy from $E_{\rm lab}=20$ MeV/nucleon to $E_{\rm lab}=60$ MeV/nucleon, the emission probabilities for high energetic δ-electrons rise by about 2 orders of magnitude, whereas almost no growth is observed when considering the results for $E_{\rm lab}=100$ MeV/nucleon. Hence the emission probabilities for high energetic δ electrons show a saturation effect with increasing beam energy. The reason for this behavior can be explained by means of the underlying stopping times, resulting from the applied nuclear trajectory. For a friction coefficient of $K=5000$ MeV fm^2 the stopping time reduces from $\tau=7.1$ fm/c to $\tau=3.6$ fm/c and to $\tau=2.8$ fm/c when increasing the beam energy according to $E_{\rm lab}=20$, 60, and 100 MeV/nucleon, respectively. Thus the bombarding energy exercises an influence on the high energetic wing of the electron spectrum only through variation of the stopping time τ.

The dependence of the emission probabilities on the nuclear friction coefficient K can also be extracted from Fig. 8. With increasing friction, i.e., shorter stopping times τ, the spectra fall off less steeply, i.e., more highly energetic electrons are emitted. For $E_{\rm lab}=60$ MeV/nucleon collisions the emission probabilities at

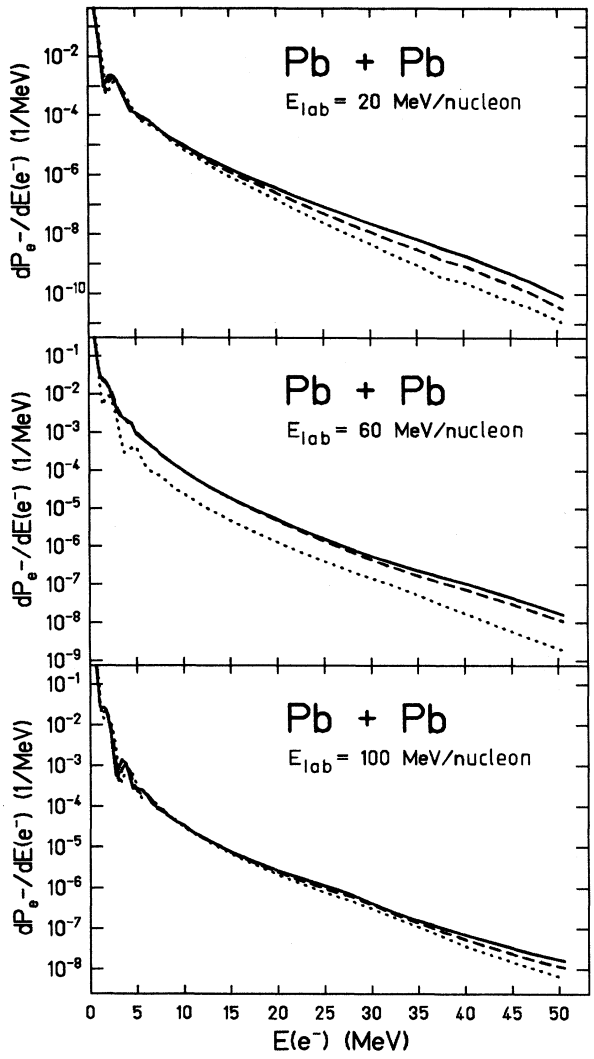

FIG. 8. Excitation probabilities of the emission of high energetic electrons in central ($b=0$) Pb+Pb collisions at the bombarding energies of $E_{\rm lab}=20$, 60, and 100 MeV/nucleon. $F=3s\sigma,4p_{1/2}\sigma$. The emission probabilities are plotted versus kinetic electron energy for different nuclear friction coefficients, i.e., $K=2500$ (dotted lines), 5000 (dashed lines), and 10000 MeV fm^2 (solid lines).

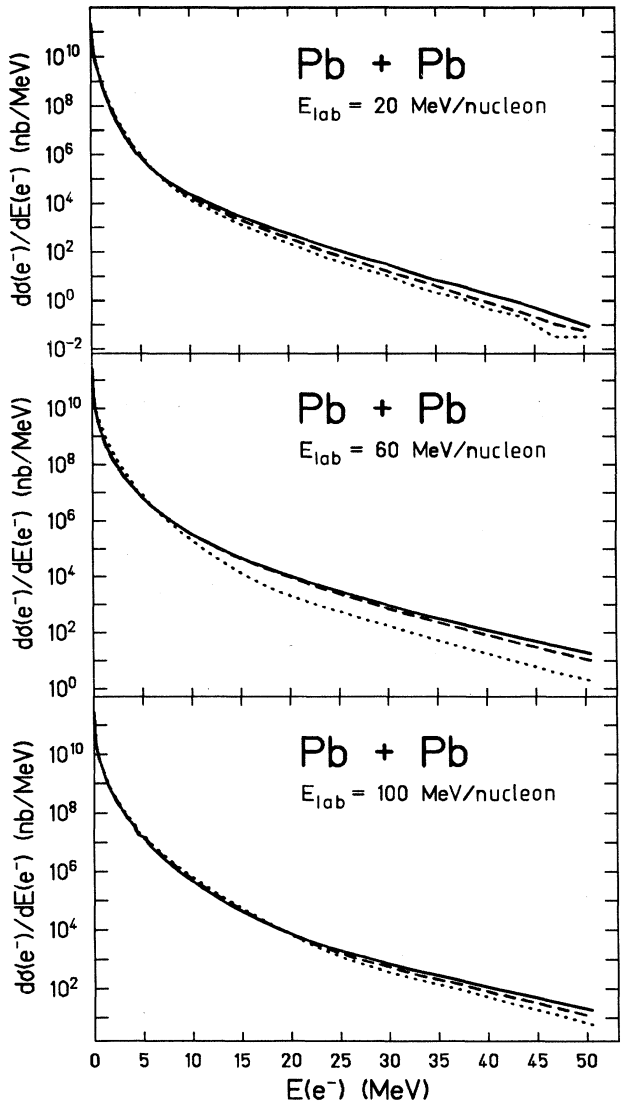

FIG. 9. Cross sections for electron emission in Pb+Pb collisions at impact parameters in the range of $b=0$ to 14 fm for beam energies $E_{\rm lab}=20$, 60, and 100 MeV/nucleon. $F=3s\sigma,4p_{1/2}\sigma$. The dependence of the spectra on the friction coefficient K is retained. The results for $K=2500$ MeV fm^2 are indicated by the dotted lines. Note the saturation of the cross section for $K=5000$ (dashed lines) and 10000 MeV fm^2 (solid lines) when increasing the beam energy from $E_{\rm lab}=60$ to 100 MeV/nucleon.

different friction coefficients differ at most by a factor of 10. In 100 MeV/nucleon collisions the stopping times vary only between $\tau=3.4$ and 2.3 fm/c for the considered friction coefficients and hence the difference between the corresponding spectra is smaller. The result of an intergration over different impact parameters from $b=0$ to $b=14$ fm for the same collisions is shown in Fig. 9. The oscillations visible in Fig. 8 for energies $E_{e^-}\leq 10$ MeV, which were caused by interference effects between the incoming and outgoing path of the Rutherford trajectory, average to zero since their position depends on the impact parameter b. The dependence of the spectral slope on the stopping time τ, however, is retained. Cross sections up to 20 nb/MeV results for the emission of electrons with a kinetic energy of $E_{e^-}=50$ MeV, so that an experimental detection could be feasible.

Up to now we have considered only the emission of electrons in intermediate energy collisions, with the crucial result that the number of electrons with high kinetic energy depends essentially on the underlying stopping time τ. In Fig. 10 we show emission probabilities of $s\sigma$-positrons in central Pb+Pb collisions at $E_{\rm lab}=60$ MeV/nucleon for a nuclear friction constant $K=5000$ MeV fm^2. In analogy to the electron emission discussed above, the excitation probabilities exhibit a larger decay

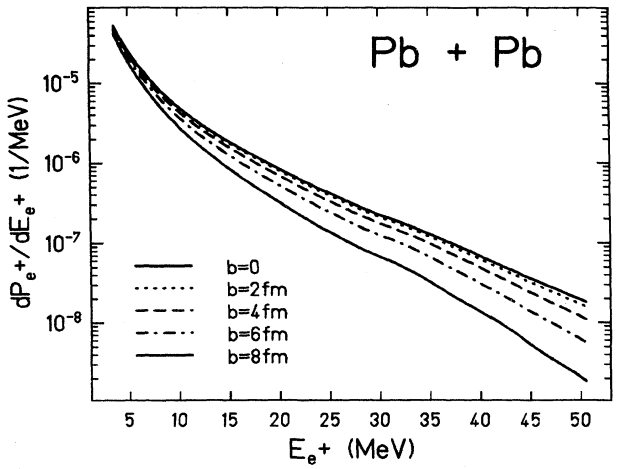

FIG. 10. Theoretical results for positron emission in 60 MeV/nucleon Pb+Pb collisions obtained by the extended coupled-channel code. The emission probabilities are displayed versus kinetic positron energies E_{e^+} for different impact parameters $b=0$, 2, 4, 6, and 8 fm and a nuclear friction constant $K=5000$ MeV fm^2. In order to save computer time, the outgoing Rutherford trajectory has been neglected and hence no oscillations are generated in the energy range $E_{e^+} \leq 10$ MeV. Only the $s\sigma$-channel contribution has been considered in these runs. $F=3_{s\sigma}$. For positron energies $E_{e^+} < 2$ MeV, the spectra exhibit a kinematic maximum similar to Fig. 1(b).

constant with increasing impact parameters b, since associated with larger stopping times τ. The systematics of the slope concerning different nuclear friction coefficients $K=2500$, 5000, and 10 000 MeV fm^2 is in close analogy to δ-electron emission. The exponential decay constant over the whole range of kinetic positron energies is notably smaller as in the comparable electron spectra. This is a consequence of the fact that for smaller kinetic energies $E_{e^\pm} \leq 5$ MeV the emission probabilities for δ electrons exceeds the corresponding values for positrons by up to 5 orders of magnitude. For high kinetic particle energies, however, the emission probabilities for δ electrons and positrons take on the same order of magnitude. The slight deflection between $E_{e^+}=30$ and 35 MeV in Fig. 10 hints at the circumstance that both, slope of the spectra and also values for the emission probabilities, are approximately of the same magnitude in δ-electron and positron spectra for sufficiently high kinetic electron or positron energies.

In principle, both the electron and positron emission processes are suited to determine the nuclear stopping time in intermediate-energy collisions. The experimental detection, however, is complicated by the small values being predicted for the emission probabilities dP_{e^+}/dE_{e^+} and dP_{e^-}/dE_{e^-} at high kinetic particle energies. Furthermore the discrimination against nonatomic direct pair creation, resulting, e.g., from neutral pion decay[40–44] $\pi^0 \rightarrow \gamma + e^+ + e^-$ might be difficult. Considering these difficulties it seems favorable to study the ratio $(dP_{e^-}/dE_{e^-})/(dP_{e^+}/dE_{e^+})$ which should decay monotonically with increasing $E_{e^\pm}$ energy and thus offers a criterion to distinguish atomic processes from particle decays with e^+, e^- emission.

V. CONCLUSIONS

In deep-inelastic heavy-ion reactions considered so far, δ-electron and positron emission have proved to be a useful tool to measure the nuclear reaction dynamics, in particular reaction times ΔT (cf. also Refs. 45–47). The latter can be defined as dwelling time in the region of nuclear overlap subtracted by the Rutherford collision time for point-like nuclei. Therefore an extended coupled-channel code has been developed, suited to evaluate emission probabilities for kinetic electron or positron energies $E_{e^\pm}$ up to 50 MeV instead of the formerly accessible limit of 2 MeV. Furthermore beam energies up to $E_{\text{lab}}=100$ MeV/nucleon can be considered now. In the present paper we have investigated two collision systems with the extended coupled-channel code. The system Th+Pb ($Z=172$) was examined with respect to δ-electron emission for kinetic energies E_{e^-} up to 10 MeV at a beam energy of $E_{\text{lab}}=8.4$ MeV/nucleon. For sufficiently narrow impact parameter windows, oscillation patterns result from coupled-channel calculations. Delay times between $\Delta T=7\times10^{-22}$ and 2.3×10^{-21} s occur for impact parameters b, varying between $b=0$ and $b=6$ fm. These values are in agreement with nuclear interaction or reaction times resulting from friction model trajectories[10,14] being defined by the time interval between the minimum and maximum of $\dot{R}/R$ subtracted by the elastic collision time. We are now in the state to describe measurements of δ-electron and positron emission in deep inelastic reactions for kinetic $e^\pm$-energies up to 10 MeV.

In the study of intermediate energy collisions the main goal is to determine the nuclear stopping time τ. As an example we have applied the extended coupled-channel code to the system Pb+Pb at 20, 60, and 100 MeV/nucleon. The nuclear trajectory was taken from a classical model with an adjustable friction coefficient. Figures 8–10 demonstrate the dependence of the high energetic wing of δ-electron and positron emission spectra on nuclear stopping time. Although the effect of different stopping times on the slope of emission probabilities versus kinetic particle energy is not so pronounced as predicted in first-order perturbation theory,[29,30] the effect still should be measurable. For Pb+Pb collisions at a bombarding energy of $E_{\text{lab}}=60$ MeV/nucleon we predict the emission of electrons with a kinetic energy of 50 MeV with a cross section of 20 nb/MeV.

We are grateful to T. Stahl for providing us with nuclear trajectories at intermediate energies.

*Present address: Hoechst AG, Abt. TEB, Postfach 800 320, D-6230 Frankfurt 80, F.R.G.

[1]J. A. Maruhn and W. Greiner, Phys. Rev. C **13**, 2404 (1976).

[2]R. Y. Cusson, R. K. Smith, and J. A. Maruhn, Phys. Rev. Lett. **36**, 1166 (1976).

[3]C. Riedel, G. Wolschin, and W. Nörenberg, Z. Phys. A **290**, 47 (1979).

[4]C. Riedel and W. Nörenberg, Z. Phys. A **290**, 385 (1979).

[5]J. Maruhn and W. Greiner, in *Treatise on Heavy-Ion Science,* edited by A. Bromley (Plenum, New York, 1985), Vol. 4, p. 565.

[6]E. M. Friedländer and H. H. Heckman, in *Treatise on Heavy-Ion Science,* edited by A. Bromley (Plenum, New York, 1985), Vol. 4, p. 403.

[7]J. R. Birkelund, J. R. Huizenga, J. N. De, and D. Sperber, Phys. Rev. Lett. **40**, 1123 (1978).

[8]J. R. Birkelund, L. E. Tubbs, J. R. Huizenga, J. N. De, and D. Sperber, Phys. Rep. **56**, 107 (1979).

[9]J. R. Birkelund and J. R. Huizenga, Annu. Rev. Nucl. Part. Sci. **33**, 265 (1983).

[10]R. Schmidt, V. D. Toneev, and G. Wolschin, Nucl. Phys. **A311**, 247 (1978).

[11]D. H. E. Gross and H. Kalinowski, Phys. Rep. **45**, 175 (1978).

[12]S. Yamaji, W. Scheid, H. J. Fink, and W. Greiner, J. Phys. G **2**, L189 (1976).

[13]K. E. Rehm, E. Essel, K. Hartel, P. Kienle, H. J. Körner, and W. Wagner, Phys. Lett. **86B**, 251 (1979).

[14]G. Wolschin, Nukleonika **22**, 1165 (1977).

[15]W. Greiner, B. Müller, and J. Rafelski, *Quantum Electrodynamics of Strong Fields* (Springer-Verlag, Berlin, 1985).

[16]J. Reinhardt, B. Müller, and W. Greiner, Phys. Rev. A **24**, 103 (1981).

[17]J. Reinhardt, U. Müller, B. Müller, and W. Greiner, Z. Phys. A **303**, 173 (1981).

[18]J. Reinhardt, B. Müller, W. Greiner, and G. Soff, Z. Phys. A **292**, 211 (1979).

[19]G. Soff, J. Reinhardt, B. Müller, and W. Greiner, Phys. Rev. Lett. **43**, 1981 (1979).

[20]U. Müller, G. Soff, J. Reinhardt, T. de Reus, B. Müller, and W. Greiner, Phys. Rev. C **30**, 1199 (1984).

[21]T. de Reus, J. Reinhardt, B. Müller, W. Greiner, U. Müller, and G. Soff, Prog. Part. Nucl. Phys. **15**, 57 (1985).

[22]G. Soff, T. de Reus, U. Müller, J. Reinhardt, B. Müller, and W. Greiner, in *Physics of Strong Fields,* Vol. 153 of *NATO Advanced Study Institute, Series B: Physics,* edited by W. Greiner (Plenum, New York, 1987), p. 81.

[23]H. Backe, P. Senger, W. Bonin, E. Kankeleit, M. Krämer, R. Krieg, V. Metag, N. Trautmann, and J. B. Wilhelmy, Phys. Rev. Lett. **50**, 1838 (1983).

[24]R. Krieg, E. Božek, U. Gollerthan, E. Kankeleit, G. Klotz-Engmann, M. Krämer, U. Meyer, H. Oeschler, and P. Senger, Phys. Rev. C **34**, 562 (1986).

[25]P. Senger, thesis, Technische Hochschule Darmstadt.

[26]P. Senger, H. Backe, M. Begemann-Blaich, H. Bokemeyer, P. Glässel, D. v. Harrach, M. Klüver, W. Konen, K. Poppensieker, K. Stiebing, J. Stroth, and K. Wallenstein, in *Physics of Strong Fields,* edited by W. Greiner (Plenum, New York, 1987), p. 423.

[27]J. Stroth, H. Backe, M. Begemann-Blaich, H. Bokemeyer, P. Glässel, D. v. Harrach, W. Konen, P. Kosmadakis, S. Mojumder, P. Senger, K. Stiebing, Nuclear contact times in dissipative heavy ion collisions measured via δ-ray spectroscopy, XXVI International Winter Meeting on Nuclear Physics, Bormio, Italy, 1987 [Ric. Sci. Ed. Educ. Perm. Suppl. **63**, 659 (1988)].

[28]M. Krämer, B. Blank, E. Božek, E. Kankeleit, G. Klotz-Engmann, C. Müntz, H. Oeschler, and M. Rhein, Phys. Lett. B **201**, 215 (1988).

[29]T. de Reus, J. Reinhardt, B. Müller, W. Greiner, U. Müller, and G. Soff, Z. Phys. A **321**, 589 (1985).

[30]T. de Reus, J. Reinhardt, B. Müller, W. Greiner, and G. Soff, Phys. Lett. **169B**, 139 (1986); Phys. Lett. B **171**, 491(E) (1986).

[31]T. de Reus, J. Reinhardt, B. Müller, W. Greiner, G. Soff, and U. Müller, J. Phys. B **17**, 615 (1984).

[32]J. Reinhardt, thesis, University of Frankfurt, 1979.

[33]J. Reinhardt, B. Müller, W. Greiner, and G. Soff, Phys. Rev. Lett. **43**, 1307 (1979).

[34]G. Soff, J. Reinhardt, B. Müller, and W. Greiner, Z. Phys. A **294**, 137 (1980).

[35]G. Soff, J. Reinhardt, W. Betz, and J. Rafelski, Phys. Scr. **17**, 417 (1978).

[36]M. E. Rose, *Relativistic Electron Theory* (Wiley, New York, 1961).

[37]C. F. Tsang, Phys. Scr. **10A**, 90 (1974).

[38]T. Stahl, M. Uhlig, B. Müller, W. Greiner, and D. Vasak, Z. Phys. A **327**, 311 (1987).

[39]C. Ngô, B. Tamain, M. Beiner, J. R. Lombard, D. Mas, and H. H. Deubler, Nucl. Phys. **A252**, 237 (1975).

[40]H. Noll, H. Dabrowski, E. Grosse, H. Heckwolf, O. Klepper, C. Michel, W. F. J. Müller, H. Stelzer, C. Brendel, W. Rösch, P. Braun-Munzinger, J. Julien, G. S. Pappalardo, G. Bizard, J. L. Laville, A. C. Müller, and J. Péter, in *Proceedings of the International Conference on Nuclear Physics,* edited by P. Blasi and R. A. Ricci (Tipografia Compositori, Bologna, 1983), Vol. 1, p. 682.

[41]H. Noll, E. Grosse, P. Braun-Munzinger, H. Dabrowski, H. Heckwolf, O. Klepper, C. Michel, W. F. J. Müller, H. Stelzer, C. Brendel, and W. Rösch, Phys. Rev. Lett. **52**, 1284 (1984).

[42]P. Braun-Munzinger, P. Paul, L. Ricken, J. Stachel, P. H. Zang, G. R. Young, F. E. Obenshain, and E. Grosse, Phys. Rev. Lett. **52**, 255 (1984).

[43]H. Heckwolf, E. Grosse, H. Dabrowski, O. Klepper, C. Michel, W. F. J. Müller, H. Noll, C. Brendel, W. Rösch, J. Julien, G. S. Pappalardo, G. Bizard, J. L. Laville, A. C. Müller, and J. Péter, Z. Phys. A **315**, 243 (1984).

[44]P. Grimm and E. Grosse, Prog. Part. Nucl. Phys. **15**, 339 (1985).

[45]Ch. Stoller, M. Nessi, E. Morenzoni, W. Wölfli, W. E. Meyerhof, J. D. Molitoris, E. Grosse, and Ch. Michel, Phys. Rev. Lett. **53**, 1329 (1984).

[46]W. E. Meyerhof and J. F. Chemin, in *Advances in Atomic and Molecular Physics,* edited by D. R. Bates and B. Bederson (Academic, New York, 1985), Vol. 20, p. 173.

[47]U. Heinz, Rep. Prog. Phys. **50**, 145 (1987).